sustainability

MDPI

Article

Multi-Objective Optimisation of Sponge City LID Facilities Incorporating Carbon Trading Mechanism

Hong Zhang and Yibing Yang *

School of Urban Economics and Management, Beijing University of Civil Engineering and Architecture, Beijing 100044, China; zhanghong@bucea.edu.cn
* Correspondence: 19170218009@163.com

Abstract

Urban stormwater management is a critical component of sustainable city development, yet conventional low impact development (LID) layout optimisation often neglects life-cycle carbon emissions and carbon-trading opportunities. This study developed an integrated multi-objective optimisation framework for sponge city LID facilities that embedded life-cycle carbon accounting and carbon trading into conventional hydrological-economic decision-making. The methodology coupled the storm water management model (SWMM) for hydrological simulation with life cycle assessment (LCA) and life cycle cost (LCC) models. The non-dominated sorting genetic algorithm III (NSGA-III) and entropy-weighted VIKOR method were utilized to solve the multi-objective problem and evaluate optimal schemes. Applied to the Fenghuangcheng pilot sponge city area in Shenzhen, China, the results showed that incorporating carbon constraints and trading drove a fundamental structural reconfiguration. The optimal layout shifted from being permeable-pavement-dominated (approximately 70%) to vegetation-based facilities. Green roofs increased to 48–50% and rain gardens to 29–41%, while permeable pavements dropped below 1%. Consequently, net life-cycle carbon emissions shifted from positive values to a net-negative balance of approximately −1.2 to −1.4 Mt CO_2e. Carbon trading revenue acted as an economic compensator, reducing net costs by up to 11%. The proposed framework provided a quantitative decision-support tool for transforming LID facilities into tradable ecological assets, supporting sustainable low-carbon sponge city planning.

Keywords: low impact development; sustainable infrastructure planning; carbon trading; sponge city; low-carbon transition

Check for updates

Academic Editor: Chi-Ming Lai

Received: 27 August 2026
Revised: 12 October 2026
Accepted: 14 October 2026
Published: 16 October 2026

Copyright: © 2026 by the authors. Licensee MDPI, Basel, Switzerland. This article is an open access article distributed under the terms and conditions of the Creative Commons Attribution (CC BY) license.

1. Introduction

The intensification of global climate change and rapid urbanisation pose multiple challenges to sustainable urban development. On the one hand, the continuous expansion of impervious surfaces exacerbates rapid runoff accumulation, leading to frequent urban flooding [1,2]. On the other hand, cities are the dominant source of carbon emissions, accounting for approximately 75% of global emissions, making low-carbon transitions an urgent imperative [3]. Within this context, low impact development (LID), which mimics natural hydrological processes through decentralised source control, has emerged as a cornerstone for both stormwater management and urban green infrastructure. Typical LID measures, such as green roofs and permeable pavements, effectively mitigate stormwater runoff while generating potential carbon benefits through ecological functions like plant carbon sequestration [4]. However, achieving the coordinated optimisation of LID selection

and spatial allocation under land, construction, and budget constraints remains a critical challenge in sustainable sponge city planning.

The methodological paradigm for LID spatial optimisation has evolved significantly, shifting from single-objective runoff control to comprehensive multi-objective frameworks that integrate spatial analysis, hydrological simulation, and evolutionary algorithms [5]. Tools like geographic information system (GIS) identify spatial suitability [6], while models such as storm water management model (SWMM) and MIKE quantify the hydrological responses of various facility combinations [7]. To navigate these complex trade-offs, algorithms like NSGA-II, NSGA-III, and multi-objective particle swarm optimization (MOPSO) have been widely applied [8,9]. Recently, advanced hybrid evolutionary algorithms, including matrix-based hybrid genetic algorithm (MBHGA), clustering-based hybrid particle swarm optimization (CBHPSO), and improved NSGA-III with hybrid crossover operators, have been proposed to enhance convergence efficiency and solution diversity in complex, high-dimensional many-objective problems [10,11]. However, existing studies often apply these methods without systematically evaluating their parameter sensitivity and robustness under carbon constraints, and most remain confined to traditional "hydrology-cost" or "hydrology-water quality-cost" frameworks, in which the low-carbon attributes and economic externalities of LID facilities are largely overlooked.

With the advancement of China's "Dual Carbon" strategy, the low-carbon attributes of LID facilities as urban green infrastructure are attracting increasing attention. LID facilities generate carbon emissions across all life-cycle stages [12], while plant-based facilities such as bioretention cells, sunken green spaces and grass swales can generate carbon reductions through plant carbon sequestration, soil carbon sinks and urban heat island mitigation [13–15]. Life Cycle Assessment (LCA) and carbon emission factor methods have become key approaches for LID carbon accounting, with studies conducted at facility, demonstration-area and urban scales [16–18]. Some studies have further explored LID structural optimisation from the perspective of synergies between pollution reduction, carbon reduction and cost-effectiveness [19]. Carbon trading mechanisms offer new avenues for realising the low-carbon value of LID. As the national carbon market matures, the carbon reduction and carbon sink benefits of green infrastructure are gradually becoming economically viable, meaning that LID facilities can function not only as engineering measures for water management but also as quantifiable and tradable ecological assets [20]. Studies on carbon trading and green infrastructure have focused on urban green spaces, forests, wetlands and ecological restoration, showing that monetisation of carbon sink value enhances economic feasibility and long-term investment returns [21]. Sun et al. [22] and Li et al. [23] have begun monetised valuation of LID carbon sink benefits, indicating that carbon revenues may offset part of construction and maintenance costs.

However, these methods have inherent limitations for LID layout optimisation and require integration. Moreover, most existing LID studies treat carbon emissions as a post-hoc indicator rather than an integrated objective, and rarely incorporate carbon trading revenues into economic evaluation. Consequently, carbon trading revenues, life-cycle carbon constraints, and hydrological targets have not been integrated into a unified multi-objective optimisation framework, leaving unclear how carbon market mechanisms drive structural shifts in LID configuration. To bridge this gap, this paper takes the Fenghuangcheng pilot area in Shenzhen, China, as a case study and proposes an integrated multi-objective optimisation framework. Its innovations are threefold: (1) integrating carbon trading revenues, life-cycle carbon emissions, and hydrological performance into a unified three-objective optimisation framework for LID layout; (2) applying parameter-tuned NSGA-III, a robust Pareto front, and entropy-weighted VIKOR decision-making to address the stochastic sensitivity of evolutionary algorithms; and (3) introducing a zero-carbon-price scenario to

isolate the effect of carbon trading revenue from that of carbon objectives and constraints. By coupling SWMM, LCC/LCA models, and NSGA-III, this study jointly considers runoff control, life-cycle carbon emissions, traditional economic costs, and carbon trading revenues. This research is of a significant importance for advancing the theoretical framework of sponge cities, providing a quantitative decision-support tool to align stormwater management with the "Dual Carbon" strategy, and ultimately fostering sustainable low-carbon urban development.

2. Methodology

Figure 1 illustrates the multi-objective optimisation workflow for LID layout design, which comprises four stages: Data Entry, Hydrological Simulation, Multi-objective Optimisation & Comparison, and Comprehensive Evaluation. In the Data Entry stage, three categories of data were prepared: basic study area data, LID parameters, and economic & environmental factors. Only the basic study area data and LID parameters were imported into the SWMM model for runoff simulation, while the economic and environmental factors were fed directly into the optimisation stage. In the Multi-objective Optimisation & Comparison stage, two models were constructed: a Traditional Optimization Model and a Low-carbon-oriented Optimization Model. Both share the Runoff Reduction Effect Model, Life Cycle Cost Model, and Life Cycle Carbon Emission Model, with objectives of maximising runoff reduction (f1), minimising net economic cost (f2), and minimising net carbon emissions (f3). The NSGA-III algorithm was applied to obtain a robust Pareto optimal solution set. Subsequently, in the comprehensive evaluation stage, multiple carbon price scenarios were analysed, and the entropy-weighted VIKOR method was used to select the optimal LID spatial layout scheme, followed by comparison with the traditional model, cross-scenario driver analysis, and sensitivity analysis of key carbon parameters.

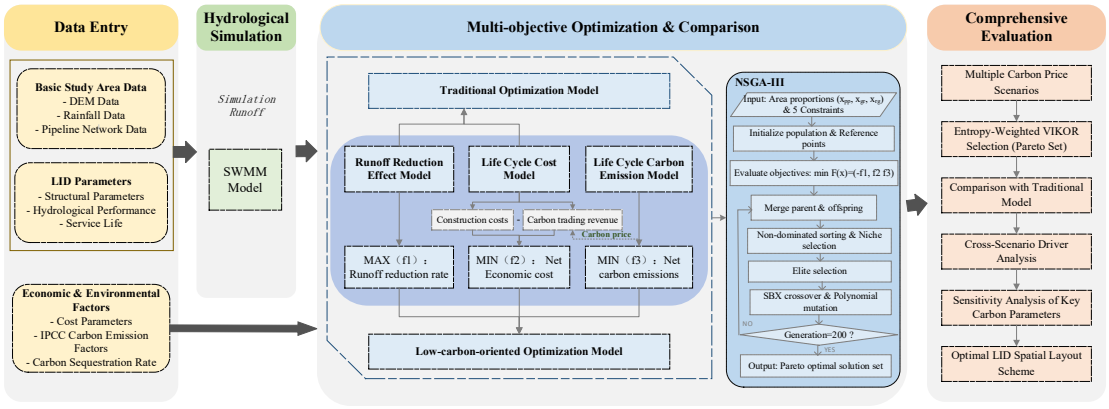


Figure 1. Research roadmap of LID facility layout optimisation under carbon trading mechanism.

2.1. Study Area

This study selected the Fenghuangcheng National Sponge City Pilot Area in Guangming District, Shenzhen, as the case study site (Figure 2), with a total area of approximately 21.86 km^2. Rainfall in this area is concentrated and exhibits distinct characteristics of short duration and high intensity, placing high demands on the runoff regulation and peak-cutting capabilities of LID facilities. The study area has gentle topography and is predominantly characterised by well-permeable soils, providing favourable baseline conditions for rainwater infiltration and retention at source. According to relevant planning atlases, the study area features a diverse range of land uses, with residential, commercial, industrial and ecological spaces interwoven; this variety of land surfaces provides a spatial foundation for the site-specific configuration of LID measures. As a national pilot site for

sponge city construction, Fenghuangcheng has already completed 55 sponge city projects, achieving significant results in runoff regulation and maintaining stable system operation. Overall, this area combines the typical spatial characteristics of a dense urban built environment with a relatively well-established foundation for sponge city construction. Accordingly, it offers reliable solutions and empirical data for optimising the spatial layout of LID facilities and for assessing the synergistic benefits arising from multiple objectives.

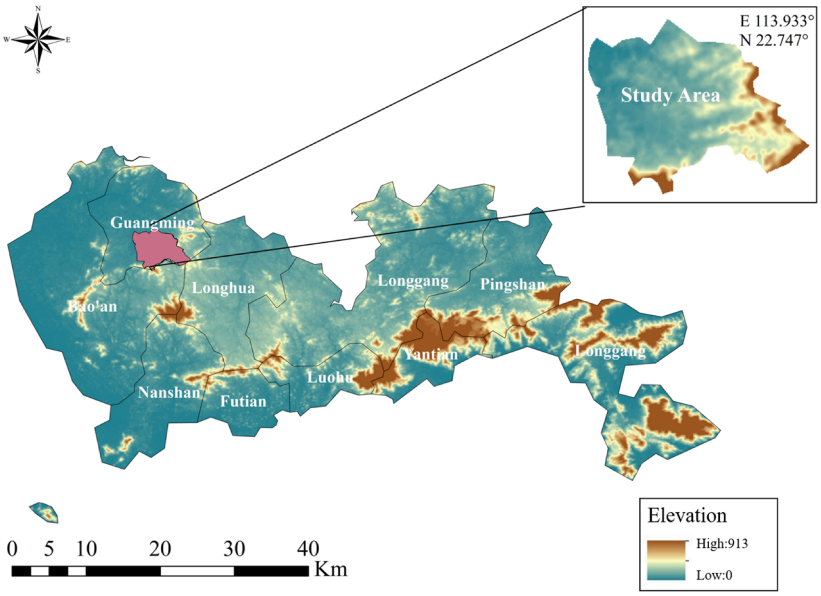


Figure 2. Topographic map of the study area.

2.2. SWMM Model

To quantitatively assess the effectiveness of LID measures in reducing urban stormwater runoff, this study developed a runoff simulation model for the study area using the Stormwater Management Model (SWMM), a stormwater modelling tool developed by the US Environmental Protection Agency (EPA) [24]. The modelling procedure included: (i) compilation of basic data; (ii) delineation of hydrological sub-basins; (iii) generalization of the drainage network topology; (iv) assignment and plausibility checking of hydrological and hydraulic parameters; (v) generation of design rainfall; and (vi) setup and simulation of LID scenarios. The spatial discretisation and drainage network topology were mainly based on two datasets: drainage network data extracted from the Atlas of the Special Plan and Implementation Scheme for Sponge City Construction in Shenzhen [25], compiled by the Shenzhen Bureau of Planning and Natural Resources; and a 30 m resolution Digital Elevation Model (DEM) from the Geospatial Data Cloud Platform. Surface routing was simulated using the nonlinear reservoir method, and conduit routing using the dynamic wave method. Model outputs included subcatchment runoff, node overflow, and outfall discharge.

For subcatchment delineation, the drainage network was first gneralized by extracting the actual pipeline routes, pipe diameters, and outfalls, forming a network topology comprising 328 nodes, 338 conduit segments, and 67 outfalls (Figure 3). DEM data were used to check node elevations and conduit slopes, ensuring consistency between the modelled flow paths and the physical drainage system. Second, Thiessen polygons were constructed based on the stormwater manhole nodes of the drainage network to automatically delineate the subcatchments in the study area [26]. Surface runoff within each subcatchment was assumed to enter the corresponding stormwater manhole node by the nearest-path principle. After delineation, the subcatchment boundaries were manually corrected according

to topography, roads, and drainage flow directions. Given the small spatial scale and gentle topography of the study area, the spatial heterogeneity of rainfall was considered negligible [27], and a single rain gauge was deployed for the entire area.



Figure 3. Hydrological sub-basins and drainage network topology. Adapted from Ref. [28].

Due to the lack of long-term observed runoff data, traditional parameter calibration against observed hydrological processes was not conducted. The SWMM parameters were initially assigned based on localised recommendations from the Shenzhen Sponge City Planning Guidelines [29], general rules from the SWMM User's Manual [30], and actual underlying surface characteristics. The Horton equation represented soil infiltration, with distinct parameters for pervious and impervious surfaces (Table 1).

Table 1. Hydrological parameters of the SWMM model.

Parameters	Values	Units
N-Imperv	0.013	
N-Perv	0.24	
Destore-Imperv	1.27	mm
Destore-Perv	3.18	mm
%Zero-Imperv	25	
Max.Infil.Rate	220	mm/h
Min.Infil.Rate	4.5	mm/h
Decay Constant	4.14	1/h
Drying Time	5	day

To assess parameter reasonableness, a composite runoff coefficient method was applied. The simulated average coefficient was 0.52, within the reasonable range (0.45–0.60) for densely built urban areas specified in GB 50014-2021 [31], indicating preliminary macro-scale consistency with local rainfall-runoff patterns. It should be noted that SWMM serves as a scenario-based simulation tool under unified assumptions to compare relative LID performance, rather than a fully calibrated predictive model. The lack of observational calibration is a limitation that may affect runoff reduction estimation and subsequent optimisation. Future studies should prioritise field monitoring for rigorous calibration and validation.

Taking into account the regional land-use characteristics and the sponge city development plan, this study selected green roofs, permeable pavements and rain gardens as the three core LID facilities for runoff regulation. To ensure the engineering practicality and

local applicability of the facility parameters, the specific design parameters for each type of LID facility are shown in Table 2. In the SWMM model, the implementation proportions of the different LID facilities were defined as decision variables for subsequent iterative simulations and performance assessment.

Table 2. Design parameters of LID facilities.

Facility Type	Layer Structure	Thickness/mm	Layer Material	Carbon Emission Factor
Green Roof	Substrate Layer	250~400	Lightweight planting soil	
	Geotextile Layer	2~4	Permeable geotextile	0.16 kg/m^2
	Drainage Layer	10~30	PVC drainage and water storage board	1765 kg/t
	Waterproofing Layer	10~20	SBS-modified bituminous root-resistant waterproofing membrane	2.37 kg/m^2
Permeable Paving	Permeable Paving Brick Layer	60~80	Permeable paving bricks	2.21 kg/m^3
	Levelling Layer	20~30	Medium-grade sand	2.51 kg/t
	Geotextile Layer	2~4	Permeable geotextile	0.16 kg/m^2
	Concrete Layer	100~150	Permeable concrete	195 kg/t
	Gravel Base Layer	150~200	Graded crushed stone	2.18 kg/t
Rain garden	Covering Layer	50~100	Crushed stone	2.18 kg/t
	Planting Soil Layer	100~1000	Planting soil	
	Filler Layer	200~1200	Fine sand	2.51 kg/t
	Drainage Layer	200~300	Gravel	6.05 kg/t
		150	Perforated collection pipe	3.6 kg/kg

Note: The physical structure parameters of LID facilities are from the Technical Guide for Sponge City Construction [32] and the Shenzhen Sponge City Design Atlas [33]. The carbon emission factors are referenced from the Technical Guidelines for Carbon Accounting and Emission Reduction in the Urban Water Sector [34], Ian et al. [35], Jie Ma [36], Singh et al. [37], Peng Cui [38], the 2022 Carbon Dioxide Emission Factors for Electricity [39], and the Standard for Building Carbon Emission Calculation [40].

For the specification of model boundary conditions, short-duration design rainfall hyetographs were generated using the Chicago storm pattern method. In accordance with the flood control and drainage standards stipulated in the Detailed Sponge City Plan for Guangming Science City, and based on the rainfall intensity formula for the western watershed of Shenzhen (Equation (1)) [41], rainfall time series with return periods of 3, 5, 10 and 20 years were calculated and generated. These design rainfall series were input into the SWMM model as meteorological data to drive multi-scenario simulations of the hydrological response and runoff reduction performance of different LID deployment schemes under each return period.

$$q = \frac{167A}{(t+b)^n} \quad (1)$$

where q is the design rainfall intensity (L·s^{-1}·hm^{-2}); t is the rainfall duration in minutes; and A, b, and n represent the rainfall intensity parameter, local constant, and storm attenuation exponent, respectively. These parameters are functions of the design return period P and are determined by the following equations (Shenzhen Meteorological Bureau et al., 2024 [41]): $A = 67.931 - 10.040 \ln(P - 0.387)$; $b = 31.178 - 1.281 \ln(P - 0.836)$; $n = 0.986 - 0.106 \ln(P - 0.247)$.

2.3. Multi-Objective Optimisation Model

2.3.1. Runoff Reduction Effect Model

To systematically quantify the hydrological performance of LID facilities, this study simulated the runoff reduction effects of different LID deployment scenarios based on the established SWMM model. For the three typical LID types mentioned above, multiple areal coverage ratios were specified and incorporated into the model to simulate hydrological processes under four design storm return periods, namely 3, 5, 10, and 20 years. Based on the simulated total runoff depth of each subcatchment from the SWMM model, the runoff reduction rate for each LID type under different areal coverage ratios was calculated using the following formula:

$$\overline{\eta_i} = \frac{1}{m}\sum_{k=1}^{m}\frac{R_{pre,0,k} - R_{lid,i,k}}{R_{pre,0,k}} \times 100\% \quad (2)$$

where $\overline{\eta_i}$ is the average runoff reduction rate for each type of LID facility; $R_{pre,0,k}$ is the total runoff depth in subcatchment k under scenarios without LID facilities (mm); $R_{lid,i,k}$ is the total runoff depth in subcatchment k under scenarios with LID facilities (mm); k is the index of the subcatchment in which LID measures are implemented; and m is the total number of subcatchments with LID facilities, m = 331.

Based on the simulation results, Python 3.12 was used to perform unified curve fitting of the datasets for each LID facility across various return periods and areal deployment ratios. The LID coverage ratio was defined as the independent variable and the runoff reduction rate as the dependent variable to characterise the hydrological responses of the facilities. Among the tested fitting forms, including linear, logarithmic, quadratic polynomial, and power functions, the power function provided the best performance, with R^2 values above 0.9 across all return periods and lower extrapolation distortion. Accordingly, the power function was adopted as the runoff reduction effect model and used in the subsequent multi-objective optimisation framework to quantify the hydrological performance of different LID combinations. Figure 4 presents the fitted relationships for the three types of LID facilities. To assess the influence of the interaction effects among LID facilities, several representative LID combinations were re-simulated using the complete SWMM model. A comparison between the runoff reduction rates derived from the full SWMM simulations and the calculated values based on the response function superposition method revealed a relative error of approximately 15%. This error was then applied as a ±15% perturbation to the runoff reduction objective of all Pareto solutions. The detailed results are provided in Section 3.4.

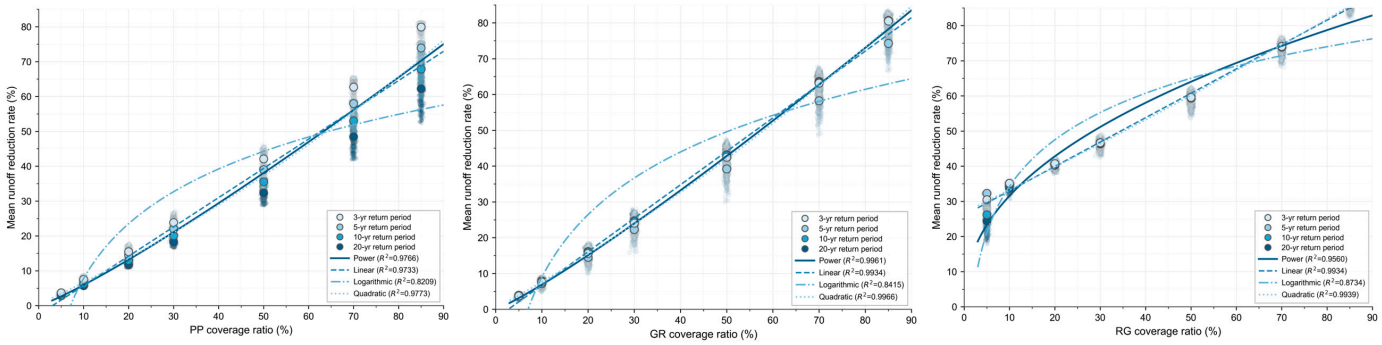


Figure 4. Fitting curves of runoff reduction efficiency for LID facilities. The grey scatter points represent the simulated data cloud under various return periods and areal deployment ratios.

2.3.2. Life Cycle Cost (LCC) Model

To assess the economic performance of each LID facility over its entire service life, this study developed a life cycle cost (LCC) model. This model not only takes into account the costs of facility construction, operation and maintenance, but also incorporates the monetised benefits corresponding to carbon effects into the calculations. For the ith type of LID facility, the life cycle cost can be expressed as:

$$E_{LCC,i} = A_{total} \times x_i \times (U_i^{con} + U_i^{om} \times T_i) + P_{carbon} \times E_{LCCE,i} \quad (3)$$

where $E_{LCC,i}$ is the total life cycle cost of the ith type of LID facility (CNY); A_{total} is the total area available for LID implementation (m^2); x_i is the area ratio of the ith LID facility; U_i^{con} is the unit construction cost (CNY/m^2); U_i^{op} is the annual operation and maintenance cost per unit area (CNY·m^{-2}·a^{-1}); T_i is the service life (a); P_{carbon} is the carbon price (CNY/t); and $E_{LCCE,i}$ is the net carbon emissions over the life cycle of the ith LID, calculated as described in Section 2.3.3. To ensure comparability across facilities with different service lives, a common assessment horizon of 30 years and a discount rate of 8% were adopted. Future operation and maintenance costs were discounted to present values. Based on Reviews and Prospects of China and World Carbon Markets (2026), the carbon price was set at 80 CNY/t. To examine the sensitivity of the optimisation results to the carbon price assumption, two additional carbon price scenarios of 50 and 150 CNY/t were established, representing anticipated decreases and increases in future carbon prices, respectively. The cost parameters of each LID facility are listed in Table 3.

Table 3. Cost parameters of LID facilities.

LID Facility Type	Construction Cost/(CNY·m^{-2})	Operation and Maintenance Cost/(CNY·m^{-2}·a^{-1})	Service Life/(a)
Green Roof	500	45	40
Permeable Paving	224	29	30
Rain Garden	700	60	30

Note: Some data are from the Investment Estimation Indicators for Sponge City Construction Projects [42], Li et al. [43], Peri et al. [44], Kavehei et al. [45].

2.3.3. Life Cycle Carbon Emissions (LCCE) Model

To quantify the carbon environmental impact of each type of LID facility throughout its life cycle, this study developed a life-cycle carbon emissions (LCCE) accounting model based on the LCA methodology [46] and the IPCC methodology [47]. The model covers carbon emissions throughout all stages of the LID life cycle, while also accounting for carbon reduction benefits associated with plant carbon sequestration, runoff reduction and the mitigation of the urban heat island effect. The net life-cycle carbon emissions of LID facilities can be expressed as:

$$E_{LCCE,i} = A_{total} \times x_i \times e_i \quad (4)$$

where $E_{LCCE,i}$ is the net life-cycle carbon emissions of the ith LID (kg CO_2-eq); A_{total} is the total area available for LID implementation; x_i is the area proportion of the ith LID; e_i is the net life-cycle carbon emissions per unit area of the ith LID (kg CO_2-eq/m^2), calculated as follows:

$$e_i = e_{pro,i} + e_{tran,i} + e_{op,i} + e_{dis,i} - e_{pl,i} - e_{ra,i} - e_{tem,i} \quad (5)$$

where $e_{pro,i}$, $e_{tran,i}$, $e_{op,i}$, $e_{dis,i}$ are the net carbon emissions of the ith LID during the material production, transport, operation and maintenance, and disposal stages, respectively (kg

CO_2-eq/m^2); $e_{pl,i}$ is the amount of carbon sequestered by plant (kg CO_2-eq/m^2); $e_{ra,i}$ is the carbon reduction from runoff mitigation (kg CO_2-eq/m^2); $e_{tem,i}$ is the carbon reduction from mitigating the urban heat island effect (kg CO_2-eq/m^2). The calculation methods for each item are as follows:

(1) Carbon emissions from material production

The production of materials required for LID facilities, such as concrete, plastics, filter media, and planting substrates, involves substantial energy consumption and associated greenhouse gas emissions during raw material extraction, processing, and manufacturing. Accordingly, material production is typically a major source of carbon emissions during the construction phase, and can be calculated by the following equation:

$$e_{pro,i} = \sum_{j=1}^{s} M_{ij} \times EF_{pro,j} \quad (6)$$

where $e_{pro,i}$ is the carbon emissions per unit area of the ith LID during material production (kg CO_2-eq/m^2); M_{ij} is the consumption per unit area of the material j used in the facility i; $EF_{pro,j}$ is the emission factor for the production stage of the material j; and s is the number of material types. The material consumption for each category is set out in Table 2.

(2) Carbon emissions from material transportation

The transportation of construction materials from production sites to the project location generates carbon emissions through fuel consumption, with the magnitude affected by transport mode, logistics conditions, and travel distance. The equation for calculating this is as follows:

$$e_{tran,i} = \sum_{j=1}^{s} M_{ij} \times D_j \times EF_{tran,j} \quad (7)$$

where $e_{tran,i}$ is the carbon emissions per unit area of the ith LID during material transportation (kg CO_2-eq/m^2); D_j is the average transport distance of the material j (km); $EF_{tran,j}$ is the emission factor for the corresponding transport mode. This study used a road transport scenario with different average transport distances set for common building materials and other materials (Table 4).

Table 4. Carbon emission parameters.

Parameter	Value	Parameter	Value
$EF_{tran,j}$ (kg CO_2-eq/(t·km))	0.129	θ_{gr} (kg CO_2-eq/(m^2·a))	0.69
D_{com} (km)	50	θ_{rg} (kg CO_2-eq/(m^2·a))	2.52
D_{om} (km)	184	μ_1 (kWh/m^3)	0.054
$EF_{op,pp}$ (kg CO_2-eq/(m^2·a))	0.07	α (kg CO_2-eq/kWh)	0.4403
$EF_{op,gr}$ (kg CO_2-eq/(m^2·a))	0.32	γ_1 (kWh/ha·a)	6.307
$EF_{op,rg}$ (kg CO_2-eq/(m^2·a))	0.15	γ_2 (kWh/ha·°C·a)	2.34
$EF_{dis,pp}$ (kg CO_2-eq/m^2)	−2	a	0.4753
$EF_{dis,gr}$ (kg CO_2-eq/m^2)	−1.7	b	0.6408
$EF_{dis,rg}$ (kg CO_2-eq/m^2)	−0.8		

Note: Data sourced from the Standard for Building Carbon Emission Calculation [40], the 2022 Carbon Dioxide Emission Factors for Electricity [39], Xiao et al. [48], She et al. [49], Keijzer et al. [50], Getter et al. [51], Cameron et al. [52], Kavehei et al. [44], Liu Wei [53].

(3) Carbon emissions from operation and maintenance

During the service life of LID facilities, routine maintenance, equipment operation, material replacement, and related energy use continuously generate carbon emissions, the amount of which is calculated by the following equation:

$$e_{op,i} = EF_{op,i} \times T_i \tag{8}$$

where $e_{op,i}$ is the carbon emissions per unit area of the ith LID during the operation and maintenance phase (kg CO_2-eq/m^2); $EF_{op,i}$ is the annual operation and maintenance emission factor per unit area; and T_i is the service life of the ith LID (a).

(4) Net carbon effect of the facility disposal stage

At the end of the service life, facility demolition, waste removal, and final disposal generate carbon emissions. Meanwhile, the recovery and reuse of recyclable materials may provide carbon offset benefits. Therefore, it can be calculated as follows:

$$e_{dis,i} = EF_{dis,i} \times S \tag{9}$$

where $e_{dis,i}$ is the carbon emissions per unit area of the ith LID during the disposal phase (kg CO_2-eq/m^2); $EF_{dis,i}$ is the emission factor of the ith LID during the disposal stage; and S is the reference area for accounting, which is set of 1 m^2 in this study.

(5) Carbon sequestration by plants

For LID facilities with plants, plants can absorb and fix atmospheric carbon dioxide through photosynthesis during growth, thereby generating ecological carbon sequestration benefits. This component can be calculated as:

$$e_{pl,i} = \theta_i T_i \tag{10}$$

where $e_{pl,i}$ is the life-cycle carbon sequestration per unit area of the ith LID (kg CO_2-eq/m^2); θ_i is the annual carbon sequestration rate per unit area (kg CO_2-eq·m^{-2}·a^{-1}); and T_i is the service life of the ith LID (a).

(6) Carbon emission reductions from runoff reduction

By reducing the volume of surface runoff discharged, LID facilities can lower energy consumption during the conveyance and treatment of rainwater, thereby generating indirect carbon emission reductions. This can be calculated as:

$$e_{ra,i} = \frac{\mu_1}{1000}(V_0 - V)\alpha \tag{11}$$

where $e_{ra,i}$ is the indirect carbon reduction per unit area of the ith LID facility resulting from runoff reduction (kg CO_2-eq/m^2); μ_1 is the conversion coefficient between runoff volume and electricity consumption; V_0 and V are the annual total runoff volumes before and after LID implementation (m^3), as simulated by the SWMM; and α is the emission factor of electricity.

(7) Carbon mitigation via urban heat island alleviation

LID facilities can indirectly generate carbon emission reduction by lowering local ambient temperatures, thereby decreasing building cooling energy demand. This reduction is calculated as:

$$e_{tem,i} = \alpha(\gamma_1 S_{GR} + \gamma_2 S_o \Delta T) T_i \tag{12}$$

$$\Delta T = a \ln S_o + b \tag{13}$$

where $e_{tem,i}$ is the carbon emissions reduction from LID facility achieved by mitigating the urban heat island effect (kg CO_2-eq/m^2); α is the electricity emission factor; γ_1 is the annual energy saving per unit green roof area (kWh/ha·a); γ_2 is the annual energy saving coefficient per unit area per degree of temperature reduction for the other two types of facilities (kWh/ha·°C·a); ΔT is the mean ambient temperature drop (°C), calculated by Equation (13); S_{GR} and S_o are the unit deployed areas of green roofs and other facilities; a and b are empirical constants; and T_i is the facility service life (a).

A one-at-a-time sensitivity analysis was conducted to evaluate the response of life-cycle carbon emission estimates to uncertainty in key parameters. Each parameter was varied by ±30% while all other parameters were held constant, and the resulting changes in net carbon emissions were quantified.

2.3.4. Multi-Objective Optimisation Based on NSGA-III

Based on the above runoff reduction effect model, life-cycle cost model, and life-cycle carbon emission model, this study constructs a multi-objective optimisation model for LID practices. The model takes the area allocation proportions of permeable pavement, green roofs, and rain gardens as decision variables. Subject to the requirements for the annual runoff control rate of sponge city construction, the spatial constraints on facility deployment, and the net carbon emission constraint, the model seeks the optimal LID combination scheme with the best hydrological performance, the lowest economic cost, and the best carbon-environmental benefit. Let x_{pp}, x_{gr}, x_{rg} be the decision variables. The model can be expressed as follows:

$$\begin{aligned} \max f_1 &= V_{pp}(x_{pp}) + V_{gr}(x_{gr}) + V_{rg}(x_{rg}) \\ \min f_2 &= E_{LCC,pp} + E_{LCC,gr} + E_{LCC,rg} \\ \min f_3 &= E_{LCCE,pp} + E_{LCCE,gr} + E_{LCCE,rg} \end{aligned} \tag{14}$$

where f_1, f_2 and f_3 denote the runoff reduction rate, life-cycle cost, and net carbon emissions of the LID combination scheme, respectively. The following constraints are imposed to satisfy both the sponge city performance targets and the practical implementation conditions:

$$s.t. \begin{cases} f_1 \geq 60\% \\ f_3 \leq 0 \\ 0 \leq x_{pp} \leq 1 \\ 0 \leq x_{gr} \leq 0.6 \\ 0 \leq x_{rg} \leq 1 \end{cases} \tag{15}$$

In the three-objective optimisation problem formulated in this study, the three objectives exhibit mutual trade-offs. This study employs NSGA-III for multi-objective optimisation because, among available multi-objective evolutionary algorithms, it is specifically designed for many-objective problems and combines non-dominated sorting with reference-point-based environmental selection, thereby achieving a better balance between convergence to the Pareto front and diversity preservation in three-objective spaces [54]. The optimisation algorithm was implemented in Python. Simulated binary crossover (SBX) and polynomial mutation (PM) were used to generate offspring solutions. To evaluate the sensitivity and robustness of the stochastic optimisation process, three parameter configurations were tested: G1, a baseline balanced-search configuration; G2, a conservative configuration emphasising local exploitation; and G3, an exploratory configuration favouring global search. The parameter settings are listed in Table 5. Each configuration was independently executed 50 times with different random seeds. Three metrics- hypervolume (HV), cardinality of Pareto front (CPF), and average Crowding Distance (ACD) were used

to evaluate the convergence and overall quality of the Pareto solution sets. HV was treated as the primary selection criterion because it jointly captures convergence and diversity, whereas CPF and ACD served as complementary diagnostics. The final configuration was selected based on the highest mean HV and the lowest HV standard deviation.

Table 5. Parameter settings of NSGA-III.

Parameter	G1	G2	G3
Population size	100	120	120
Number of generations	200	200	200
Crossover probability	0.8	0.9	0.9
Crossover distribution index	15	25	10
Mutation probability	0.05	0.03	0.1
Mutation distribution index	20	30	15

2.4. Entropy-Weighted VIKOR Integrated Decision-Making Model

To screen for representative solutions with decision-making value from the set of Pareto-optimal solutions generated by NSGA-III, the entropy-weighted VIKOR integrated model is employed for evaluation and ranking of the Pareto-front solutions, so as to identify the LID combination scheme with the best overall performance. First, an initial evaluation matrix is constructed using all non-dominated solutions within the Pareto solution set. Then, the entropy weight method is employed to assign objective weights based on the degree of dispersion of each indicator. Finally, the VIKOR method is used to determine the compromise solution. This model can effectively handle scheme selection under multi-objective conflict conditions and has strong applicability and robustness.

In this study, runoff reduction rate, life-cycle cost, and life-cycle net carbon emissions are selected as evaluation indicators, with the first being a benefit-type indicator and the latter two being cost-type indicators. To eliminate the influence of dimensional differences, the raw data are standardised as follows:

$$r_{ij} = \frac{x_{ij} - \min(x_j)}{\max(x_j) - \min(x_j)} (Benefit - type\ indicator) \tag{16}$$

$$r_{ij} = \frac{\max(x_j) - x_{ij}}{\max(x_j) - \min(x_j)} (Cost - type\ indicator) \tag{17}$$

In terms of weight determination, this study adopts the entropy weight method to calculate the objective weights of the indicators according to their degree of dispersion in the Pareto solution set. The proportion, information entropy and objective weight for the jth indicator are calculated respectively, as follows:

$$p_{ij} = r_{ij} / \sum_{i=1}^{m} r_{ij} \tag{18}$$

$$e_j = -\frac{1}{\ln(m)} \sum_{i=1}^{m} p_{ij} \ln(p_{ij}) \tag{19}$$

$$w_j = (1 - e_j) / \sum_{j=1}^{n} (1 - e_j) \tag{20}$$

After obtaining the indicator weights, the VIKOR method is employed to comprehensively rank the Pareto solution set. Let f_j^* and f_j^- denote the positive and negative ideal solutions, respectively, of the jth objective in the original matrix. Combined with

the weights w_j obtained by the entropy weight method, the group utility value S_i and the individual regret value R_i of the ith scheme are calculated as follows:

$$S_i = \sum_{j=1}^{n} w_j \frac{f_j^* - y_{ij}}{f_j^* - f_j^-} \tag{21}$$

$$R_i = \max_j \left[w_j \frac{f_j^* - y_{ij}}{f_j^* - f_j^-} \right] \tag{22}$$

A comprehensive ranking index is further constructed as follows:

$$Q_i = v \frac{S_i - S^*}{S^- - S^*} + (1 - \mathrm{v}) \frac{R_i - R^*}{R^- - R^*} \tag{23}$$

where S^* and S^- are the minimum and maximum values of S_i, respectively; R^* and R^- are the minimum and maximum values of R_i, respectively; and v is the decision mechanism coefficient, taken as 0.5, which is used to balance group utility and individual regret. The schemes are ranked in ascending order according to the value of Q_i. A smaller Q_i value indicates that the scheme is closer to the ideal solution and thus has better overall performance.

3. Results

3.1. Pareto Solution Set Based on Multi-Objective Optimisation

This study employed the NSGA-III algorithm to solve the multi-objective optimisation problem for the combined layout of LID facilities. To ensure the reliability of the optimisation process, the performance of three distinct search strategies (G1, G2, and G3) was quantitatively assessed. Statistical results show that G3 achieved the highest mean Hypervolume (HV = 0.7404, SD = 0.0029), outperforming G1 (HV = 0.7380, SD = 0.0039) and G2 (HV = 0.7371, SD = 0.0049). It also obtained the highest Pareto front cardinality (CPF = 47.70), while its average crowding distance (ACD = 0.1264) remained stable and comparable to those of G1 and G2. These metrics collectively demonstrate that G3 provides superior algorithmic convergence, diversity, and robustness. Meanwhile, Kruskal–Wallis tests indicated significant differences in HV among the three configurations (p = 0.002), and pairwise Mann–Whitney U tests confirmed that G3 significantly outperformed both G1 and G2. Consequently, the robust Pareto front generated by the G3 configuration was selected for all subsequent analyses.

Figure 5 presents the three-dimensional distribution of the Pareto solution set, intuitively revealing the trade-off relationships among the three objectives. A pronounced non-linear trade-off exists between hydrological performance and economic investment: as runoff reduction increases from approximately 60% to nearly 99%, net cost rises continuously, with marginal cost steepening significantly at higher performance tiers. Achieving 60–75% runoff reduction requires only 800–1200 CNY/m^2, whereas exceeding 90% escalates costs to 1800–2400 CNY/m^2. Net carbon emissions, represented by the Z-axis and color gradient, conflict with economic cost but align synergistically with runoff reduction. Economical configurations yield minimal carbon mitigation (about 0.0–0.4 Mt CO_2e), while deep decarbonisation below −1.2 Mt CO_2e demands investments exceeding 1800 CNY/m^2. Enhanced runoff reduction also drives greater carbon sink capacity. Structurally, Pareto solutions form discrete bands along the runoff axis, indicating that within similar hydrological intervals, various LID configurations can produce substantial differences in cost and carbon footprints.

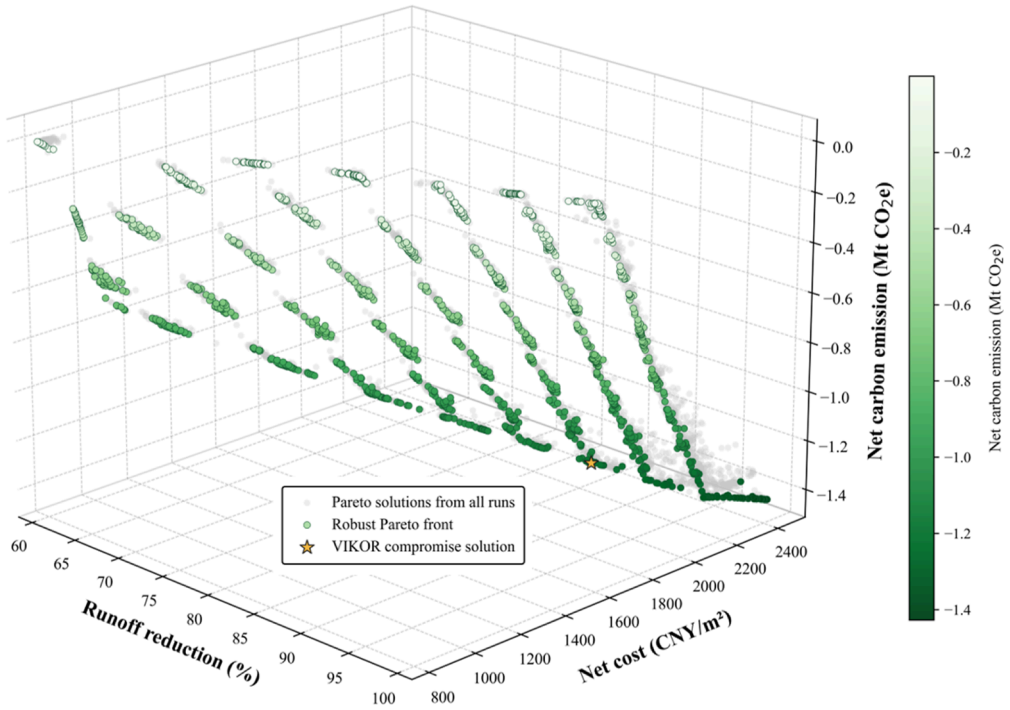


Figure 5. Three-dimensional distribution of the robust Pareto solution set.

3.2. Comparison of Optimisation Results Between the Conventional and Carbon Trading Policy Models

To clarify the impact of the carbon trading mechanism on the optimisation results, this study compares a conventional model without carbon constraints and a carbon-constrained model incorporating carbon trading revenue, using 80 CNY/t CO_2 as the baseline carbon price (Figure 6). Both scenarios can achieve runoff reduction rates exceeding 60%; however, their performance in terms of net cost and net carbon emissions differs markedly. In the scenario without carbon constraints, the Pareto solutions are concentrated in a relatively low net cost range (680–1130 CNY/m^2) and exhibit a relatively gentle, approximately linear increasing trend as the runoff reduction rate increases. Nevertheless, most solutions in this scenario exhibit high positive net carbon emissions, approximately 0.9–1.1 Mt CO_2e. Conversely, the carbon-constrained model restricts solutions to a negative net carbon emission region. In this context, negative net carbon emissions represent an ideal accounting outcome in which the carbon sequestration provided by LID facilities and the carbon reductions from their environmental benefits exceed the life-cycle carbon emissions. Driven by this constraint, some solutions approach −1.4 Mt CO_2e. At an equivalent unit cost, this translates to an average decrease of 118.2% in net carbon emissions compared to traditional model. However, these environmental benefits come at a substantial financial cost: relative to the traditional model, at the same runoff reduction rate, the carbon-constrained model increases unit cost by 58.7% on average. This indicates that the introduction of carbon constraints and carbon trading revenue alters the feasible solution space, requiring optimisation to simultaneously coordinate runoff reduction, life-cycle cost, and carbon trading revenue.

Figure 7 further illustrates pronounced differences in LID facility combinations under the two orientations. In the conventional-oriented schemes, permeable pavement accounts for a relatively high proportion, with most schemes approaching its maximum feasible share under the total area constraint, whereas green roofs and rain gardens account for relatively low proportions. After introducing carbon constraints, the allocated proportions of green roofs and rain gardens increase substantially. At the benchmark carbon price of

80 CNY/t CO_2e, the mean share of green roofs rises from 0.001% in the conventional model to 35.73%, and the mean share of rain gardens increases from 5.18% to 22.51%. Notably, the proportion of rain gardens exhibits a wider distribution range across the Pareto solutions than that of green roofs, indicating greater configurational flexibility. In contrast, the proportion of permeable pavement becomes more dispersed and is significantly lower than its near-upper-limit state in the conventional model. These results indicate that incorporating carbon performance and carbon trading benefits into the optimisation drives the model to favour facility combinations with lower life-cycle carbon emissions or stronger carbon sequestration benefits, shifting LID configuration strategies from an economically cost-dominated mode to an integrated ecological optimisation mode that coordinates runoff control, economic investment, and carbon emission reduction.

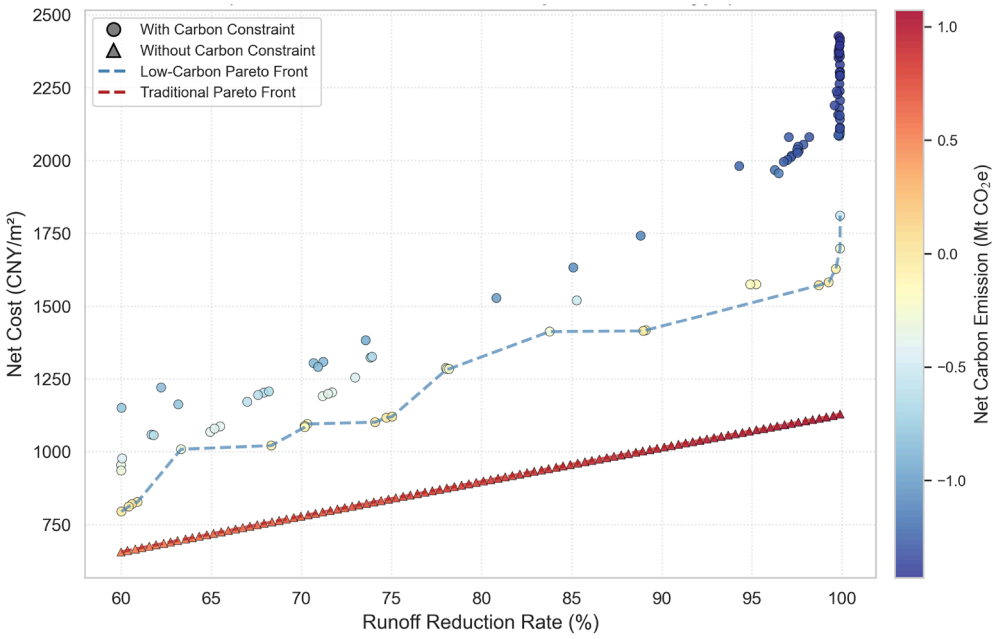


Figure 6. Comparison of Pareto solution sets for two scenarios.

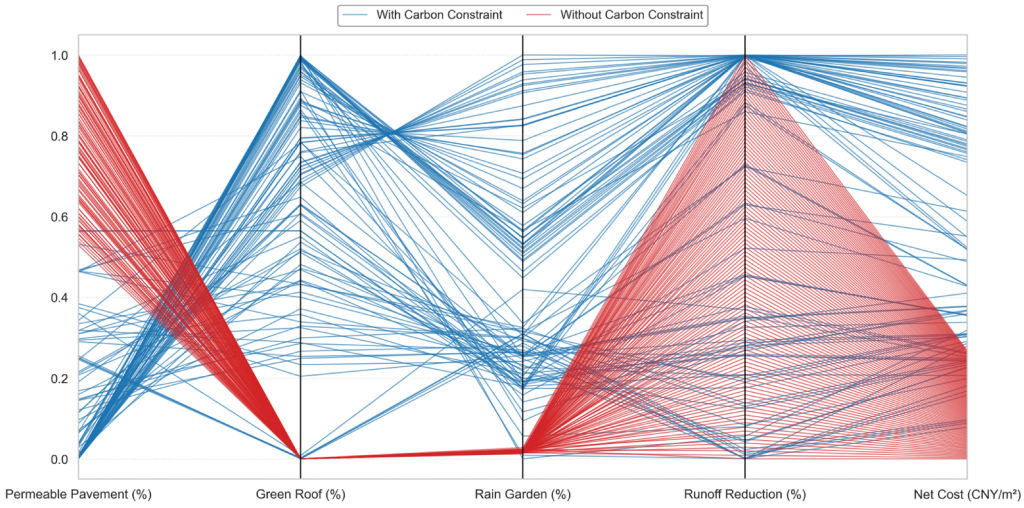


Figure 7. Comparison of LID layout schemes under two scenarios.

3.3. Effects of Carbon Price Variation on LID Facility Configuration

To evaluate the effects of carbon-price variation on optimal LID configurations, four carbon-price scenarios were examined: 0, 50, 80, and 150 CNY/t CO_2e. The Pareto solution sets obtained under each scenario were ranked using the entropy-weighted VIKOR

method. Table 6 presents the LID area proportions and multi-objective performance of the two highest-ranked compromise solutions under each scenario.

Table 6. Top-2 VIKOR compromise solutions under traditional and carbon trading scenarios.

Scenario	Carbon Price (CNY/t)	PP (%)	GR (%)	RG (%)	Runoff Reduction (%)	Net Cost (CNY/m^2)	Net Carbon (Mt CO_2e)	Q
Traditional		70.88	0.01	4.59	79.37	890.39	0.82	0.384
		70.32	0.01	4.66	78.99	885.93	0.81	0.384
Carbon trading	0	0.21	49.42	39.27	99.90	2120.66	−1.31	0.076
	0	1.15	49.28	38.81	99.89	2116.36	−1.29	0.080
	50	0.03	49.84	33.63	96.45	1984.41	−1.24	0.084
	50	0.08	49.05	39.84	99.86	2121.93	−1.31	0.085
	80	0.02	49.76	29.48	93.35	1877.08	−1.19	0.085
	80	0.01	48.56	35.77	96.69	2006.56	−1.25	0.086
	150	0.02	49.05	37.01	98.00	2044.27	−1.28	0.070
	150	0.12	48.14	41.26	99.88	2130.15	−1.32	0.071

Note: PP = permeable pavement; GR = green roof; RG = rain garden. Q is the VIKOR ranking index. The objective weights determined by the entropy method for runoff reduction, net cost, and net carbon emissions were w_1 = 0.38, w_2 = 0.41, and w_3 = 0.21, respectively.

Compared with the traditional model, LID configurations changed substantially once carbon-related elements were introduced. In the traditional solutions, permeable pavement dominated, accounting for 70.88% and 70.32% of the LID area, while green roofs were almost absent and rain gardens accounted for only 4.59% and 4.66%. In contrast, under all carbon-price scenarios, green roofs became the dominant measure, with area proportions consistently ranging from 48.14% to 49.84%. Permeable pavement declined sharply to below 1.2%, and rain gardens increased to 29.48–41.26%. Net carbon emissions shifted from positive values in the traditional model to negative values under carbon constraints.

To isolate the fundamental effect of the carbon trading mechanism from the impact of carbon price fluctuations, a baseline scenario with a carbon price of 0 CNY/t CO_2e was introduced. Compared with the traditional model, the LID configuration under this zero-carbon-price scenario still exhibited a consistent shift trend, despite the absence of a carbon price signal. This indicates that the structural transformation of the LID layout is primarily driven by the inclusion of carbon footprint accounting as an intrinsic optimisation objective, rather than by direct financial incentives alone. Furthermore, comparing the 0 CNY/t baseline with the 50, 80, and 150 CNY/t scenarios reveals the explicit economic role of actual carbon pricing. The introduction of active carbon trading effectively lowered the net cost of the LID systems. Notably, compared with the 0 CNY/t scenario, the net cost was reduced by up to 11.49%. Therefore, the carbon trading mechanism mainly acts as an economic incentive, while the low-carbon transition of LID configurations is robust across the examined carbon-price range.

To examine the robustness of the VIKOR-based decision, sensitivity analyses were conducted by perturbing the VIKOR coefficient v (±5%) and the entropy-derived weights of the three objectives (±10%). The results showed that in all cases, the Spearman rank correlation coefficients between the original and perturbed rankings remained above 0.99, indicating a high degree of consistency in the overall ranking. Although the rankings of the optimal solutions occasionally changed, the preferred LID configuration remained dominated by green roofs and rain gardens, and the carbon-reduction-driven transition trend persisted. These findings suggest that the VIKOR-based decision is generally robust to perturbations in parameters and weights.

3.4. Uncertainty and Sensitivity of Carbon Emissions and Runoff Reduction

Figure 8 presents the effects of ±30% perturbations in key carbon emission parameters on total life-cycle carbon emissions. Overall, the model is relatively insensitive to variations in most emission factors associated with the operation and end-of-life stages, with the resulting changes in total carbon emissions generally remaining below 6%. In particular, the emission factor for the operational stage of permeable pavement and the end-of-life emission factors of all facilities exerted the smallest influence, producing changes of only 0–1%.

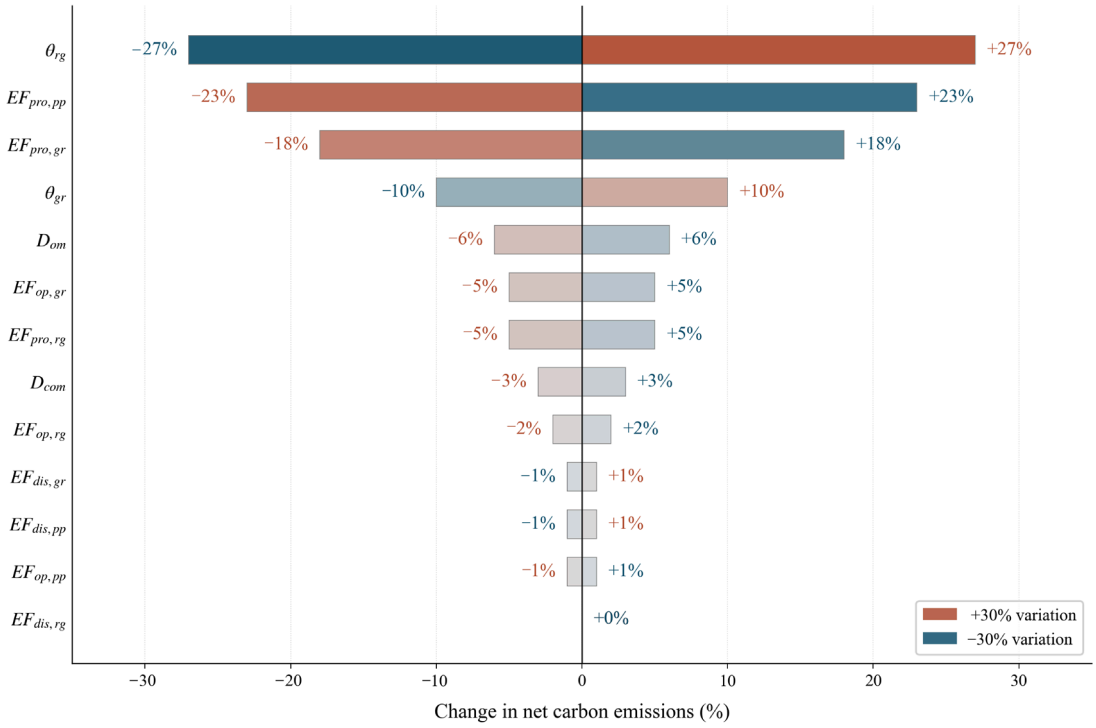


Figure 8. Parameter sensitivity of net carbon emissions in the life-cycle carbon accounting model.

In contrast, the annual carbon sequestration rate of rain gardens (θ_{rg}), the material-production-stage emission factor of permeable pavement ($EF_{pro,pp}$), and that of green roofs ($EF_{pro,gr}$) exhibited relatively high sensitivity. Under ±30% perturbations, θ_{rg} generated the largest variation in total carbon emissions, reaching 27%, whereas the carbon sequestration rate of green roofs (θ_{gr}) resulted in a moderate change of approximately 10%. These findings indicate that the life-cycle carbon emission results are generally robust; however, vegetation carbon sequestration rates and material-production-stage emission factors for LID facilities represent the primary sources of model uncertainty.

Furthermore, the influence of runoff reduction uncertainty was examined. The complete SWMM simulation of representative LID combinations showed a relative error of approximately 15% in runoff reduction compared with the response-function superposition method. Applying a ±15% perturbation to the runoff objective and re-performing non-dominated sorting, the resulting Pareto fronts remained consistent in terms of LID proportion ranges (green roofs 48–50%, rain gardens 29–41%, permeable pavement < 1.2%), and the carbon-price-driven low-carbon transition trend was preserved. These results indicate that the main optimisation conclusions are robust to the uncalibrated SWMM model and LID interaction effects.

4. Discussion

4.1. Trade-Offs and Synergy Mechanisms Among Multiple Objectives

The multi-objective optimisation results reveal a pronounced nonlinear trade-off among the runoff reduction rate, life-cycle cost, and net carbon emissions, which jointly define the optimisation boundary of LID facility combinations. The Pareto front distribution shows that as the runoff reduction target increases, the cost exhibits a clear pattern of increasing marginal increments. This indicates that continuously increasing LID facility coverage does not necessarily produce proportional improvements in hydrological benefits. Once runoff control performance has reached a relatively high level, further improving the reduction rate may require higher-cost facilities or a substantial expansion of the LID construction scale. Therefore, if the runoff reduction rate alone is used as the basis for scheme selection, investment costs may become excessively high.

The synergy between runoff reduction and carbon mitigation is rooted in the multi-functional nature of vegetation-based LID facilities. Green roofs and rain gardens not only attenuate runoff but also sequester carbon through plant biomass and soil organic matter, mitigate urban heat islands, and substitute for carbon-intensive grey infrastructure. These co-benefits explain why scenarios with higher runoff reduction generally exhibit lower net carbon emissions. However, these ecological benefits require higher initial investment and more intensive maintenance, creating a trade-off between carbon performance and economic cost. This confirms that LID facilities should be understood as hybrid infrastructure integrating hydrological, ecological, and carbon functions, rather than as purely drainage measures.

4.2. Synergistic Impacts of Carbon Constraints and Carbon Pricing on LID Configuration Pathways

When transitioning from the conventional model to the carbon-constrained model, the optimal LID configuration undergoes a significant structural reconfiguration: the layout shifts from being dominated by permeable pavement to being dominated by green roofs and rain gardens. In the conventional optimisation framework, permeable pavement possesses strong economic attractiveness due to its lower unit cost and large applicable area. However, its material production and construction phases generate substantial embodied carbon. When life-cycle carbon emissions are internalised as an optimisation objective and a non-positive carbon constraintis is applied, the relative competitiveness of permeable pavement diminishes abruptly. Although green roofs and rain gardens require higher initial capital, they provide long-term carbon sequestration and reduce reliance on high-carbon grey infrastructure, thus securing a structural advantage within the carbon-constrained decision space.

The net-negative carbon balance obtained under the carbon-constrained formulation is the carbon-accounting manifestation of this structural reconfiguration. Specifically, the negative values arise mainly from three sources: (1) direct carbon sequestration by vegetation and soil media in green roofs and rain gardens; (2) avoided emissions from substituting LID facilities for traditional high-carbon grey infrastructure; and (3) indirect carbon reductions from environmental co-benefits, such as building energy savings through urban heat island mitigation. It is important to note that these negative values represent a physical carbon balance and are driven primarily by the carbon objective and the non-positive carbon constraint, rather than by carbon trading revenue.

The role of carbon trading revenue is different. By partially offsetting the additional cost of low-carbon configurations, it reduces the net cost relative to the zero-carbon-price baseline, but it cannot fully close the economic gap with the conventional model. Carbon pricing thus acts as a synergistic economic compensator. The forced adoption of

vegetation-rich configurations inevitably raises initial capital expenditures; however, the carbon trading mechanism effectively internalizes the aforementioned physical negative emissions into upfront economic cash flows, thereby buffering the economic shock of the green transition. Sensitivity analysis further reveals different configurational elasticities: green roofs maintain structural rigidity across all carbon prices owing to their combined spatial and environmental benefits, whereas rain gardens serve as the elastic variable, dynamically balancing strict hydrological targets and budgetary limits under varying carbon market signals.

4.3. Implications for Urban LID Planning and Low-Carbon Development

At the planning level, the results suggest that LID allocation should be guided by an integrated assessment of hydrological performance, economic cost, and life-cycle carbon performance. Conventional sponge city planning that focuses primarily on runoff control and construction cost may underestimate the environmental burden of carbon-intensive materials and overlook the long-term carbon benefits of vegetation-based facilities. Incorporating carbon performance as a core constraint can steer planning toward configurations that are more aligned with dual-carbon goals.

At the implementation level, differentiated strategies are needed. New development areas and ecologically sensitive zones can prioritise green roofs and rain gardens, which offer strong carbon sequestration and runoff control, even though they require higher initial investment. Existing built-up areas or financially constrained districts may adopt a phased approach: initially combining permeable pavement with rain gardens to meet runoff control requirements, then gradually increasing green roof coverage as fiscal capacity allows. This stepwise strategy balances hydrological performance, economic feasibility, and carbon reduction.

At the policy and management levels, the findings support the inclusion of life-cycle carbon performance in sponge city evaluation systems. Carbon trading revenue can partially offset the additional cost of low-carbon configurations, but it should be complemented by fiscal subsidies, green finance, and performance-based incentives. Long-term monitoring of vegetation growth and carbon sequestration, together with the development of localised emission-factor databases, is essential for reducing uncertainty and supporting evidence-based decision-making. Overall, the transition from conventional engineering control to low-carbon hybrid infrastructure requires not only technical optimisation but also institutional and financial innovation.

5. Conclusions

This study develops an integrated multi-objective optimisation framework for Sponge City LID facilities, embedding life-cycle carbon accounting and carbon trading into conventional hydrological-economic decision-making. Using the Fenghuangcheng pilot area as a case study, the following conclusions are drawn.

Carbon objectives drive a fundamental structural reconfiguration of LID layouts. Under the conventional framework, the optimal configuration is dominated by permeable pavement, with green roofs almost absent and rain gardens accounting for only about 5%. This layout is economically attractive but yields positive net life-cycle carbon emissions. Once carbon constraints and trading revenues are internalised, the layout shifts markedly towards vegetation-based facilities: green roofs increase to about 48–50% and rain gardens to about 29–41%, while permeable pavement drops below 1%. This shift enables a net-negative carbon balance of approximately -1.2 to -1.4 Mt CO_2e. The negative value arises from vegetation and soil carbon sequestration, avoided emissions from substituting grey infrastructure, and indirect reductions from heat island mitigation.

Carbon trading acts as an economic compensator, while the low-carbon transition is primarily driven by carbon objectives and constraints. Carbon trading revenue partially offsets the additional cost of low-carbon configurations, reducing the net cost by up to about 11% relative to the zero-carbon-price baseline, but it cannot fully close the gap with the conventional model. Carbon price sensitivity analysis across 0–150 CNY/t CO_2e shows that the preferred configuration remains structurally stable. This indicates that the low-carbon transition is driven mainly by life-cycle carbon targets and constraints rather than by short-term carbon price fluctuations. VIKOR sensitivity analysis further confirms the robustness of the decision, with Spearman rank correlations exceeding 0.99 and the low-carbon configuration trend persisting under most weight perturbations.

The proposed framework provides a quantitative decision-support tool for integrating stormwater management with China's "Dual Carbon" strategy, transforming LID facilities into theoretically tradable ecological assets. However, several limitations remain. Due to the lack of long-term observed hydrological data, the SWMM model parameters were not rigorously calibrated, which may introduce uncertainties into the absolute quantification of runoff reduction. Furthermore, the carbon price was treated under static scenarios, whereas real-world carbon markets are highly volatile. Additionally, the current framework assumes these carbon benefits are theoretically eligible for trading without accounting for practical market frictions, such as project registration, transaction, and verification costs. Future research should prioritise field-scale monitoring to validate and calibrate the hydrological and carbon accounting models. Additionally, integrating dynamic carbon pricing forecasting models, incorporating practical transaction costs for comprehensive economic feasibility assessments, and exploring the spatial heterogeneity of carbon sinks across diverse urban microclimates will further refine the optimisation framework for sustainable Sponge City development.

Author Contributions: H.Z.: Writing—original draft, Supervision, Writing—review and editing; Y.Y.: Writing—original draft, Data curation, Software, Methodology. All authors have read and agreed to the published version of the manuscript.

Funding: This research received no external funding.

Data Availability Statement: The original contributions presented in the study are included in the article.

Conflicts of Interest: The authors declare no conflicts of interest.

References

1. Fletcher, T.D.; Burns, M.J.; Russell, K.L.; Hamel, P.; Duchesne, S.; Cherqui, F.; Roy, A.H. Concepts and evolution of urban hydrology. *Nat. Rev. Earth Environ.* **2024**, *5*, 789–801. [CrossRef]
2. Shafique, M.; Kim, R.; Kim, K.-H. Rainfall runoff mitigation by retrofitted permeable pavement in an urban area. *Sustainability* **2018**, *10*, 1231. [CrossRef]
3. Srivastava, C.; Bharat, A. Unlocking urban resilience potential of a city through comprehending carbon-thermal emission scenarios. *Nat. Hazards* **2025**, *121*, 19355–19385. [CrossRef]
4. Boongaling, C.G.K.; Sevilla-Nastor, J.B.; Espaldon, M.V.O.; Sanchez, P.A.J.; Villanueva-Peyraube, J.D.; Jago-on, K.A.B. Assessment of low impact development (LID) strategies under different land uses in an urban sub-catchment in the Philippines. *J. Environ. Manag.* **2024**, *369*, 122328. [CrossRef] [PubMed]
5. Chiu, Y.-J.; Chang, L.-C.; Lin, Y.-T.; Lin, Y.-T.; Liu, C.-W.; Lee, J.-J. Hydrologic performance assessment of low impact development facilities based on monitoring data and SWMM modeling in an urban catchment in Taiwan. *Sci. Rep.* **2025**, *15*, 27251. [CrossRef] [PubMed]
6. Şenocak, İ.; Şimşek, G.; Afshar, M.H.; Tuna, A.; Alp, S.Ç.; Bektaş, H.O.; Alp, E. A multi-scale framework for assessing the suitability of low impact development in a dense flood-prone urban area. *Int. J. Disaster Risk Reduct.* **2025**, *130*, 105873. [CrossRef]
7. Yin, D.; Zhang, X.; Jia, H.; Xu, L.; Jia, Q.; Yang, Y. A new framework to assess and optimize urban flood resilience with green-grey-blue system. *J. Hydrol.* **2025**, *651*, 132614. [CrossRef]

8. Tang, S.; Jiang, J.; Shamseldin, A.Y.; Shi, H.; Wang, X.; Shang, F.; Wang, S.; Zheng, Y. Comprehensive optimisation framework for low impact development facility layout design with cost−benefit analysis: A case study in Shenzhen City, China. *ACS ES T Water* **2022**, *2*, 63–74. [CrossRef]
9. Wang, J.; Liu, J.; Wang, H.; Mei, C. Approaches to multi-objective optimisation and assessment of green infrastructure and their multi-functional effectiveness: A review. *Water* **2020**, *12*, 2714. [CrossRef]
10. Akopov, A.S. MBHGA: A matrix-based hybrid genetic algorithm for solving an agent-based model of controlled trade interactions. *IEEE Access* **2025**, *13*, 26843–26863. [CrossRef]
11. Ma, L.; Zou, D. An improved NSGA-III with hybrid crossover operator for multi-objective optimisation of complex combined cooling, heating, and power systems. *Energy Sci. Eng.* **2025**, *13*, 1509–1543. [CrossRef]
12. Ma, Y.; Liu, X.; Liu, J.; Du, C.; Liang, M.; Li, W.; Cao, L.; Wang, D.; Wang, H.; Zhang, T.; et al. Carbon emission accounting and reduction evaluation in sponge city residential areas. *Water* **2024**, *16*, 2535. [CrossRef]
13. Ho, C.-C.; Su, Y.-Q.; Chiang, P.-C. Comprehensive evaluation of the hydrology, pollutant removal, and carbon sequestration performance of biochar-enriched bioretention soil. *Sci. Total Environ.* **2026**, *1011*, 181174. [CrossRef]
14. Jiang, C.; Zhang, Y.; Zhang, X.; Han, Q.; Xiao, Y. Research on the carbon profit and loss correlation mechanism of sponge city construction life cycle in urban built up areas. *Ecohydrol. Hydrobiol.* **2025**, *25*, 126–137. [CrossRef]
15. Moore, T.L.C.; Hunt, W.F. Ecosystem service provision by stormwater wetlands and ponds—A means for evaluation? *Water Res.* **2012**, *46*, 6811–6823. [CrossRef] [PubMed]
16. Chai, H.; Xu, C.; Peng, S.; Xia, Y.; Zhao, H.; Gong, Y. Unlocking the carbon mitigation potential of green infrastructure: Evidence from China's Sponge City Program. *Environ. Sci. Technol.* **2026**, *60*, 5479–5491. [CrossRef] [PubMed]
17. Tang, S.; Yan, X.; Jiang, J.; Zheng, Y.; Yang, Y.; Xu, P.; Shang, F. Catchment-scale life cycle impacts of green infrastructures and sensitivity to runoff coefficient with stormwater modelling. *Sci. Total Environ.* **2023**, *904*, 166736. [CrossRef] [PubMed]
18. Liu, X.F.; Li, H.; Wang, D.Q.; Chen, H.; Liu, J.L.; Li, W.; Cao, L.B.; Zhang, T.T.; Wei, B.G. Low-carbon layout optimisation of community LID facilities based on response surface methodology. *Environ. Eng.* **2024**, *42*, 115–130. (In Chinese) [CrossRef]
19. Chang, W.; Liu, G.; Chen, Y.; Huo, Z.; Fang, D.; Agostinho, F.; Almeida, C.M.V.B.; Giannetti, B.F. Assessing inter-industrial ecosystem service flows and economic benefits of sponge city: A comprehensive input-output analysis. *Environ. Impact Assess. Rev.* **2025**, *114*, 107955. [CrossRef]
20. Liu, Q.; Xiong, K.; Chen, Y.; Feng, M. Advancements in ecological assets and ecological product supply: In-depth insights from Karst World Heritage sites. *Herit. Sci.* **2024**, *12*, 398. [CrossRef]
21. Limb, B.J.; Quinn, J.C.; Johnson, A.; Sowby, R.B.; Thomas, E. The potential of carbon markets to accelerate green infrastructure based water quality trading. *Commun. Earth Environ.* **2024**, *5*, 185. [CrossRef]
22. Sun, H.; Gao, P.C.; Wang, H.; Fang, D.L. Multi-objective optimisation and benefit analysis of spatial layout of low impact development facilities based on stormwater management model and NSGA-II. *J. Beijing Norm. Univ. (Nat. Sci.)* **2025**, *61*, 238–246. (In Chinese)
23. Li, Z.; Xu, C.; Zhou, Z.; Sun, M.; Hu, X.; Li, X.; Jia, H.; Lu, P.; Hou, J. Bridging LCA and urban construction quotas: A novel framework for sponge city infrastructure in semi-arid China. *Environ. Impact Assess. Rev.* **2026**, *117*, 108208. [CrossRef]
24. Gironás, J.; Roesner, L.A.; Rossman, L.A.; Davis, J. A new applications manual for the Storm Water Management Model (SWMM). *Environ. Model. Softw.* **2010**, *25*, 813–814. [CrossRef]
25. Shenzhen Planning and Natural Resources Bureau. Atlas of the Special Planning and Implementation Plan (Optimized) for Shenzhen Sponge City Construction. 2019. Available online: https://pnr.sz.gov.cn/gkmlpt/content/5/5841/post_5841591.html#4281 (accessed on 13 April 2025).
26. Han, D.; Bray, M. Automated Thiessen polygon generation. *Water Resour. Res.* **2006**, *42*, W11502. [CrossRef]
27. Terink, W.; Leijnse, H.; van den Eertwegh, G.; Uijlenhoet, R. Spatial resolutions in areal rainfall estimation and their impact on hydrological simulations of a lowland catchment. *J. Hydrol.* **2018**, *563*, 319–335. [CrossRef]
28. Zhang, H.; Yang, Y.B. Multi-Objective Optimization of Spatial Layout of Sponge City LID Facilities under Carbon Constraints. *Acta Sci. Circumstantiae.* **2026**, *46*, 520–532. (In Chinese) [CrossRef]
29. Shenzhen Planning and Natural Resources Bureau. Announcement on the Publication of the Shenzhen Sponge City Planning Essentials and Review Guidelines. 2019. Available online: https://pnr.sz.gov.cn/ywzy/ghzs/content/post_5841595.html (accessed on 13 April 2025).
30. Rossman, L.A.; Simon, M.A. *Storm Water Management Model User's Manual Version 5.2*; U.S. Environmental Protection Agency: Washington, DC, USA, 2022. Available online: https://www.epa.gov/system/files/documents/2022-04/swmm-users-manual-version-5.2.pdf (accessed on 13 April 2025).
31. *GB 50014-2021*; Standard for Design of Outdoor Wastewater Engineering. China Planning Press: Beijing, China, 2021.
32. Ministry of Housing and Urban-Rural Development of the People's Republic of China. *Technical Guide for Sponge City Construction-Construction of Low Impact Development Stormwater System*; China Architecture & Building Press: Beijing, China, 2014.

33. *DB4403/T 24-2019*; Design Drawings for Sponge City Facilities. Shenzhen Administration for Market Regulation: Shenzhen, China, 2019.
34. Hao, X.; Liu, R. *Guidelines for Carbon Accounting and Emission Reduction in the Urban Water Sector*; IWA Publishing: London, UK, 2024.
35. Ian, C.; John, K.; Cui, Y.Z. Evaluation of embodied carbon of conventional pavement and permeable concrete brick pavement. *Build. Blocks Block Build.* **2012**, *2012*, 32–35+25. (In Chinese)
36. Ma, J. Carbon Source Analysis and Carbon Emission Research of Typical Sponge City Construction Measures. Master's Thesis, Shanxi Agricultural University, Jinzhong, China, 2019. Available online: https://kns.cnki.net/KCMS/detail/detail.aspx?dbcode=CMFD&dbname=CMFD201901&filename=1019021258.nh (accessed on 20 March 2025). (In Chinese)
37. Singh, A.; Vaddy, P.; Biligiri, K.P. Quantification of embodied energy and carbon footprint of pervious concrete pavements through a methodical lifecycle assessment framework. *Resour. Conserv. Recycl.* **2020**, *161*, 104953. [CrossRef]
38. Cui, P. Construction and Application Research of Building Life Cycle Carbon Emission Factor Library. Master's Thesis, Southeast University, Nanjing, China, 2015. Available online: https://https-kns-cnki-net-443.door.bucea.edu.cn/kcms2/article/abstract?v=jit-Bskw5eT5IdgWsD9M3RUJ2CKfZP4znGv4n9wpk9hG7-ZxlN-ErkfU9qpZDq_Lm_MMsojFQ-2ZCjr8i3rkJqY9ELL2Roxp6GgA1a3zqzAv3AwT2efmg4zz-8fCqu_2Znk7hCxKXJrcT8Wdbdkg2lzv61Xq1RLdnqBY_4-2L9rH2z1yN5eE_g==&uniplatform=NZKPT&language=CHS (accessed on 15 March 2024). (In Chinese)
39. Ministry of Ecology and Environment of the People's Republic of China; National Bureau of Statistics of China. Announcement on the Release of 2022 Carbon Dioxide Emission Factors for Electricity. 2024. Available online: https://www.mee.gov.cn/xxgk2018/xxgk/xxgk01/202412/t20241226_1099413.html (accessed on 11 May 2025).
40. *GB/T 51366-2019*; Standard for Building Carbon Emission Calculation. China Architecture & Building Press: Beijing, China, 2019.
41. Shenzhen Meteorological Bureau; Shenzhen Planning and Natural Resources Bureau; Shenzhen Water Authority. *Shenzhen Rainfall Intensity Formula and Calculation Charts by Watershed*; Shenzhen Meteorological Bureau: Shenzhen, China, 2024.
42. *ZYA1-02(01)-2018*; Investment Estimation Indicators for Sponge City Construction Projects. China Planning Press: Beijing, China, 2018.
43. Li, Y.; Huang, J.J.; Hu, M.; Yang, H.; Tanaka, K. Design of low impact development in the urban context considering hydrological performance and life-cycle cost. *J. Flood Risk Manag.* **2020**, *13*, e12625. [CrossRef]
44. Peri, G.; Traverso, M.; Finkbeiner, M.; Rizzo, G. The cost of green roofs disposal in a life cycle perspective: Covering the gap. *Energy* **2012**, *48*, 406–414. [CrossRef]
45. Kavehei, E.; Jenkins, G.A.; Adame, M.F.; Lemckert, C. Carbon sequestration potential for mitigating the carbon footprint of green stormwater infrastructure. *Renew. Sustain. Energy Rev.* **2018**, *94*, 1179–1191. [CrossRef]
46. *ISO 14040:2006*; Environmental Management—Life Cycle Assessment—Principles and Framework. International Organization for Standardization: Geneva, Switzerland, 2006.
47. Intergovernmental Panel on Climate Change. *2006 IPCC Guidelines for National Greenhouse Gas Inventories*; Intergovernmental Panel on Climate Change: Geneva, Switzerland, 2006. Available online: https://www.ipcc-nggip.iges.or.jp/public/2006gl/ (accessed on 24 January 2025).
48. Xiao, X.Q.; She, D.X.; Xia, J.; Zhang, X.; Xu, Z.X. Carbon emission accounting of Shenzhen sponge demonstration area based on full life cycle. *Water Resour. Prot.* **2025**, *41*, 222–231. (In Chinese)
49. She, L.; Wei, M.; You, X.-Y. Multi-objective layout optimisation for sponge city by annealing algorithm and its environmental benefits analysis. *Sustain. Cities Soc.* **2021**, *66*, 102706. [CrossRef]
50. Keijzer, E.E.; Leegwater, G.A.; de Vos-Effting, S.E.; de Wit, M.S. Carbon footprint comparison of innovative techniques in the construction and maintenance of road infrastructure in The Netherlands. *Environ. Sci. Policy* **2015**, *54*, 218–225. [CrossRef]
51. Getter, K.L.; Rowe, D.B.; Andresen, J.A. Quantifying the effect of slope on extensive green roof stormwater retention. *Ecol. Eng.* **2007**, *31*, 225–231. [CrossRef]
52. Cameron, R.W.F.; Blanuša, T.; Taylor, J.E.; Salisbury, A.; Halstead, A.J.; Henricot, B.; Thompson, K. The domestic garden—Its contribution to urban green infrastructure. *Urban For. Urban Green.* **2012**, *11*, 129–137. [CrossRef]
53. Liu, W. Runoff Reduction and Carbon Emission Accounting Research of Park Sponge Facilities Based on SWMM. Master's Thesis, Anhui Jianzhu University, Hefei, China, 2025. (In Chinese) [CrossRef]
54. Deb, K.; Jain, H. An evolutionary many-objective optimisation algorithm using reference-point-based nondominated sorting approach, Part I: Solving problems with box constraints. *IEEE Trans. Evol. Comput.* **2014**, *18*, 577–601. [CrossRef]

Disclaimer/Publisher's Note: The statements, opinions and data contained in all publications are solely those of the individual author(s) and contributor(s) and not of MDPI and/or the editor(s). MDPI and/or the editor(s) disclaim responsibility for any injury to people or property resulting from any ideas, methods, instructions or products referred to in the content.